

Electronic structure and magneto-optical Kerr effect of Tm monochalcogenides

V. N. Antonov* and B. N. Harmon
 Ames Laboratory, Iowa State University, Iowa, 50011

A. N. Yaresko
 Max Planck Institute for Physics of Complex Systems, D-01187 Dresden, Germany
 (Received 29 November 2000; published 2 May 2001)

The optical and magneto-optical (MO) spectra of Tm monochalcogenides are investigated theoretically from first principles, using the fully relativistic Dirac linear combination of muffin-tin orbitals band structure method. The electronic structure is obtained with the local-spin-density approximation (LSDA), as well as with the so-called LSDA+ U approach. In contrast to LSDA, where the stable solution in TmTe is a metal, the LSDA+ U gave an insulating ground state. LSDA+ U theory predicts the thulium ion in TmTe to be in an integer divalent state. It also shows a gradual decreasing of the energy gap with reducing of the lattice constant. LSDA+ U theoretical calculations produce a similar energy band structure in TmS and TmSe, with twelve $4f$ bands fully occupied and hybridized with chalcogenide p states. The 14th f hole level was found to be completely unoccupied and well above the Fermi level and a hole 13th f level is partly occupied and pinned at the Fermi level. The occupation number of the 13th f level is equal to 0.12 and 0.27 in TmS and TmSe, respectively (valence 2.88+ and 2.73+). Such an energy band structure of thulium monochalcogenides describes well their measured bremsstrahlung isochromat spectroscopy (BIS), and x-ray and ultraviolet photoemission spectra as well as the optical and MO spectra. The origin of the Kerr rotation realized in the compounds is examined.

DOI: 10.1103/PhysRevB.63.205112

PACS number(s): 71.28.+d, 75.30.Mb

I. INTRODUCTION

Determination of the energy band structure of solids is a many-body problem. Band theory, a mean-field theory to treat this problem, in the framework of the local-spin-density approximation (LSDA), has been successful for many kinds of materials, and has become the *de facto* tool of first-principle calculations in solid state physics. It has contributed significantly to the understanding of material properties at the microscopic level. However, there are some systematic errors that have been observed when using the LSDA. In particular, the LSDA fails to describe the electronic structure and properties of f -electron systems in which the interaction among the electrons are strong. A wide variety of physical properties arise from the correlations among f electrons: metal-insulator transitions, valence fluctuations in the Kondo effect, heavy-fermion behavior, superconductivity, and so on. These are now called strongly correlated electron systems and many new concepts to address these phenomena have been constructed. However, the understanding of these systems is not complete.

The Tm monochalcogenides TmS, TmSe, and TmTe constitute a well-known family of strongly correlated electron systems. They form a very interesting group of materials in which many characteristic phenomena are expressed. In the series of the Tm monochalcogenides one has the interesting possibility to go from integer trivalent metallic TmS to integral divalent semiconducting TmTe through intermediate valence TmSe.¹⁻³ The unique feature of thulium compounds compared with intermediate valence materials containing cerium, samarium, or europium is that both ground-state configurations of thulium have a nonzero magnetic moment. TmS exhibits antiferromagnetic order, which is an almost

type-II sinusoidally modulated structure below $T_N=6.2$ K.⁴ It has been classified as a Kondo lattice compound due to a metallic resistivity, which increases Kondo-like down to about 15 K.⁵⁻⁸ TmSe has attracted interest because of the valence fluctuation between $4f^{12}$ and $4f^{13}$ configurations, Kondo effects, antiferromagnetic order, and a possible metal-insulator transition. This compound has the peculiarity that two magnetic valence states Tm^{2+} and Tm^{3+} are involved in the valence fluctuation. Evidence comes from photoemission experiments,^{2,9-14} and also from measurements related to magnetic properties, resistivity, and specific heat.¹⁵⁻¹⁹ However, the situation is so complicated that there is no overall consistent explanation of the physical properties of this compound. The resistivity of TmSe shows a Kondo-like logarithmic temperature dependence at high temperatures followed by a sharp increase at $T_N=3.5$ K, which is thought to be a transition into an insulating state.^{18,20,21} This anomaly in the vicinity of T_N shows a very complicated response to external magnetic fields and to pressure.^{17,22}

TmTe is a magnetic semiconductor with a localized 13th f level between a filled Te5 p valence band and an empty Tm5 d conduction band.² The lattice constant and the Curie constant show that the Tm ions are divalent at ambient pressure.¹ TmTe is interesting in its own right, especially since it was recently reported²³ to undergo a phase transition at $T_Q=1.7$ K, far above the magnetic ordering temperature ($T_N\sim 0.2-0.4$ K depending on the specimen). This transition was ascribed to the onset of long-range ordering among the Tm quadrupolar moments, but the exact mechanism is still controversial.²⁴

The pressure effects on transport properties of TmTe were investigated by Matsumura *et al.*²⁵ It was found that at room temperature, the resistivity of TmTe with increasing pressure

showed an exponential decrease up to 2 GPa, indicating a linear closing of the energy gap (with $d\Delta/dP = -207 \text{ meV/GPa}$), followed by an almost pressure-independent metallic regime. The resistivity in the metallic regime showed a logarithmic temperature dependence reminiscent of the Kondo effect, and a TmSe-like anomaly appeared at low temperature and above 5 GPa. At 5.7 GPa the resistivity showed an abrupt decrease that corresponded to a structural phase transition.

The resistivity of TmSe under pressure up to 8 GPa and below room temperature has been measured in Ref. 24. At low temperatures below about 10 K, the pressure dependence of the resistivity shows two maxima; one occurring at about 1 GPa, where the magnetic phase transition takes place, and the other at about 7 GPa. The measurements of the magnetic susceptibility of TmSe up to 350 K under 1 GPa showed that the application of pressure increases the $\text{Tm}^{3+}/\text{Tm}^{2+}$ ratio. This result suggests that the increase in $|d\rho/d \ln T|$ is due to an increase in the hybridization between the localized Tm $4f$ states and the conduction electrons with pressure. The behavior of TmSe below about 3 GPa is similar to that of TmTe in the metallic phase between 2 and 5.7 GPa.⁶ In TmS, the slope $|d\rho/d \ln T|$ decreased with pressure,⁶ which resembles the behavior of TmSe above 3 GPa. It should also be mentioned that TmSe shows a strong dependence of valence structure and transport properties depending on stoichiometry and the sample quality.³

Spectroscopically, the electronic structure of Tm monochalcogenides has been investigated experimentally by means of photoemission,^{2,9-13} resonance photoemission,¹⁴ point contact spectroscopy,²⁶ x-ray absorption spectroscopy,²⁷ x-ray bremsstrahlung isochromat spectroscopy²⁸ (BIS) and optical²⁸⁻³⁰ and magneto-optical (MO) spectroscopy.³¹⁻³³

Photoelectron spectroscopy in the x-ray and ultraviolet ranges (XPS and UPS) provide information on the energy position of Tm^{2+} and $\text{Tm}^{3+}4f$ states in TmX ($X = \text{S, Se, Te}$) compounds. Structures in UPS and XPS spectra with a binding energy between 0 and 6 eV were identified to be the multiplet structures of the $4f^{12}$ final states and the structures between 6 and 17 eV to be the multiplet structures of the $4f^{11}$ final states.^{2,9-14} A recent resonant photoemission study of Tm monochalcogenides gives an estimated mean valence equal to 2.91 for TmS, 2.79 for TmSe, and 2.15 for TmTe.¹⁴

To our best knowledge, the optical and magneto-optical properties of Tm monochalcogenides have not yet been calculated theoretically using first principles, although band-structure calculations for TmSe were performed in Ref. 34 by means of the self-consistent full-potential linear augmented plane-wave (FLAPW) method with the local-density approximation. Total energy versus volume calculations were performed. The resulting value of the lattice constant, $5.68 \pm 0.01 \text{ \AA}$ was in good agreement with the experimental value $5.69 \pm 0.02 \text{ \AA}$, while the value for the bulk modulus, $68 \pm 10 \text{ GPa}$, was almost twice the experimental number $35 \pm 10 \text{ GPa}$. The LDA bulk modulus can be significantly improved by shifting the f levels 40 mRy downwards. Such shifts are not unexpected since the LDA is known to place the energies of $4f$ states incorrectly relative to other states

due to improper treating of the correlation effects. The correlated nature of $4f$ electrons in TmSe was taken into account with the so-called LDA++ method in Ref. 35. The authors calculated the total density of states in the TmSe compound to compare it with the experimental XPS spectrum.

The aim of this work is the theoretical study of the electronic structure and optical and magneto-optical spectra of TmX ($X = \text{S, Se and Te}$). We also investigated theoretically the electronic structure and optical and MO properties of $\text{TmSe}_{1-x}\text{Te}_x$, $\text{Tm}_{0.5}\text{Eu}_{0.5}\text{Se}$, and $\text{Tm}_{0.5}\text{Y}_{0.5}\text{Se}$ systems. This is motivated by the fact that although a large number of investigations have been devoted to the experimental study of the photoemission, BIS, optical and MO spectra of Tm monochalcogenides,^{2,9-14,28-33} there is no coherent picture concerning the microscopic origin of the MO spectra and the electronic structure. In particular, the energy position of $4f$ states and valency of Tm ions in these compounds are of interest. As an example we can mention that the valency of the Tm ion in TmSe was found to be 2.75+ determined from the lattice constant,¹ 2.56+, 2.53+, and 2.64+ from the Curie constant³ (depending from the sample quality and the temperature conditions), 2.79+ and 2.68+ from the recently measured total yield (TY) (absorption) and off-resonance UV photoemission spectra, respectively.¹⁴

This paper may be considered as the next in the series of our previous papers,³⁶⁻³⁹ where we investigated the electronic structure and MO properties of the chromium spinel chalcogenides,³⁶ neodymium chalcogenides,³⁷ uranium chalcogenides and pnictides,³⁸ and the metal-insulator transition (MIT) compound Fe_3O_4 .³⁹ It was shown that MO spectra are very useful for drawing conclusions about the appropriate model description. The density-functional theory in the local-spin-density approximation gives a fully satisfactory explanation of the MO Kerr spectra of transition-metal compounds and alloys in most cases, while the MO spectra of $4f$ compounds and the MIT compounds Fe_3O_4 are best described using the LSDA+ U approach.

The paper is organized as follows. Section II presents a description of the crystal structure of the Tm monochalcogenides and the computational details. Section III is devoted to the electronic structure and optical and MO properties of the Tm monochalcogenides calculated in the LSDA and LSDA+ U approximations. The optical and MO theoretical calculations are compared to the experimental measurements. Finally, the results are summarized in Sec. IV.

II. CRYSTAL STRUCTURE AND COMPUTATIONAL DETAILS

The application of plain LSDA calculations to f -electron systems is often inappropriate because of the correlated nature of the f shell. To account better for the on-site f -electron correlations, we have adopted the LSDA+ U approach as a suitable model.⁴⁰

A rigorous formulation for the quasiparticle properties of solids is the Green-function approach.⁴¹ The self-energy $\Sigma = G_0^{-1} - G^{-1}$ of the single-particle Green function G is energy dependent and yields the correlation corrections to the

single-particle (mean-field) approximation to the quasiparticle excitation spectrum described by G_0 . With a number of plausible assumptions, the LSDA+ U approach has been related to the so-called GW approximation^{42,43} to Σ in Ref. 44. Already the simplest random-phase approximation applied to Σ for the Hubbard model yields a jump of $\Sigma(E)$ at the Fermi level E_F by the Hubbard U . The more elaborate analysis of Ref. 44 results in a correlation correction to the mean-field approximation of the self-energy, which is $U_{\text{eff}}/2$ downward below the Fermi level and $U_{\text{eff}}/2$ upward above the Fermi level. As mean-field theory in a crystal always describes a delocalized situation and the LSDA Kohn-Sham potential is a well-proven approximation to the self-energy for weakly correlated systems,⁴² the suggestion is

$$\sum (\mathbf{r}, \mathbf{r}'; E) \approx \delta(\mathbf{r} - \mathbf{r}') V_{\text{LSDA}}(\mathbf{r}) + P_m \frac{U_{\text{eff}}}{2} \times [\theta(E - E_F) - \theta(E_F - E)] P_m, \quad (1)$$

where P_m is the projector onto a strongly correlated m state.

The LSDA+ U approach simply uses Eq. (1) to replace the LSDA Kohn-Sham potential in the self-consistency loop. This can be considered as a rough approximation to Σ . Since the potential shift is taken to be constant in space, it does not deform the Kohn-Sham orbital ϕ_m . However, it shifts the levels of strongly correlated motion away from the Fermi level and thus removes incorrect hybridization with conduction states, which would spoil the calculated ground-state spin density. On the other hand, being understood as an approximation to Σ , it hopefully yields for the Kohn-Sham band structure the same quality of a working approximation to the quasiparticle excitation spectrum as it does in the case of weakly correlated metals. Estimates for U_{eff} may be obtained from constrained density functional calculations or from GW calculations in which case the approach is parameter-free. Most reliable are those results that do not vary sensitively depending on the value of U_{eff} within a certain reasonable range.

The LSDA+ U method has proved to be an efficient and reliable tool for calculating the electronic structure of systems where the Coulomb interaction is strong enough to cause localization of the electrons (for a review see Ref. 44). The LSDA+ U approach was recently applied to the heavy-fermion compounds YbPtBi (Ref. 45) and Yb₄X₃ ($X = \text{P}, \text{As}, \text{Sb}, \text{and Bi}$),⁴⁶ and was able to describe the MO properties of CeSb,⁴⁷ neodymium chalcogenides,³⁷ and the metal-insulator transition compound Fe₃O₄.³⁹

Tm monochalcogenides crystallizes in the NaCl-type crystal structure, and the space group is $Fm\bar{3}m$ (No. 225). In our band-structure calculations we used the experimentally measured constants ($a = 5.42, 5.69, \text{and } 6.346 \text{ \AA}$) for TmS, TmSe, and TmTe respectively.⁴⁸

The details of the computational method are described in our previous papers,^{36,37} and here we only mention several aspects. The electronic structure of the compounds was calculated self-consistently using the local-spin-density approximation⁴⁹ and the fully relativistic spin-polarized LMTO method in the atomic-sphere approximation, includ-

ing the combined correction (ASA+CC).^{41,50-53} Core-charge densities were recalculated at every iteration of the self-consistency loop. The combined correction terms have been included also in calculation of the optical matrix elements.⁵⁴ We have calculated the absorptive part of the optical conductivity in a wide energy range. The Kramers-Kronig transformation has been used to calculate the dispersive parts of the optical conductivity from the absorptive parts. To improve the potential we include additional empty spheres in the $8c$ positions. The basis consisted of the Tm $s, p, d, f,$ and g ; S, Se, and Te $s, p,$ and $d,$ and empty sphere s and p LMTO's. The energy expansion parameters $E_{v,RI}$ were chosen at the centers of gravity of the occupied parts of the partial densities of states both for charge density calculations and for MO calculations. The \mathbf{k} -space integrations were performed with the improved tetrahedron method⁵⁵ and charge self-consistency was obtained with 1330 irreducible \mathbf{k} points.

We have adopted the LSDA+ U method⁴⁰ as a different level of approximation to treat the electron-electron correlation. The Hubbard-like U_{eff} usually is evaluated by comparison of theoretically calculated energy positions of f bands with XPS and UPS measurements. From photoemission measurements U_{eff} is found to be in the range of 5 to 7 eV for Tm compounds.⁵⁶ Optical measurements estimate the U_{eff} for TmS as $5.3 \pm 0.2 \text{ eV}$.²⁹ The estimated U_{eff} as the difference between the centroids of the Tm³⁺ and Tm²⁺ x-ray photoemission spectra yields $U_{\text{eff}} = 6.6$ and 7.4 in TmSe and TmTe, respectively.¹⁰ It can be also calculated from atomic Dirac-Hartree-Fock⁵⁶ (DHF) or from Green-function impurity calculations⁵⁷ and from band-structure calculations in the supercell approximation.⁵⁸ The DHF calculation gives $U_{\text{eff}} \approx 6.5 \text{ eV}$ and our calculations of U_{eff} in the supercell approximation give $U_{\text{eff}} = 6.2 \text{ eV}$ for TmS. The calculated value of U_{eff} can depend strongly on theoretical approximations, and it may be better to regard the value of U_{eff} as a parameter and try to specify it from comparison of the calculated physical properties with experiments. We found that the best agreement between calculated and measured MO spectra can be achieved with $U_{\text{eff}} = 6 \text{ eV}$.

It is still not clear how to choose the projections of the orbital momentum onto the spin direction m_l if we have more than one occupied state. The value of the magnetic moment and MO spectra strongly depends on the m_l 's and it may be better to regard the values of m_l 's as a parameters and try to specify them from comparison of the calculated physical properties with experiment. We performed calculations for every possible combination of the m_l 's and found that the best agreement between calculated and measured optical and MO spectra can be achieved with $m_l = \pm 2$ for Tm³⁺ in TmS and TmSe. These values give also total magnetic moments equal to $2.45\mu_B$ and $2.32\mu_B$ for TmS and TmSe respectively. The experimentally measured magnetic moment for type-I antiferromagnetic TmSe is equal to $(1.7 \pm 0.2)\mu_B$ from Ref. 59 and $\sim 2.5\mu_B$ from Ref. 60.

III. RESULTS AND DISCUSSION

A. TmS

In our optical and MO calculations we have performed three independent fully relativistic spin-polarized band-

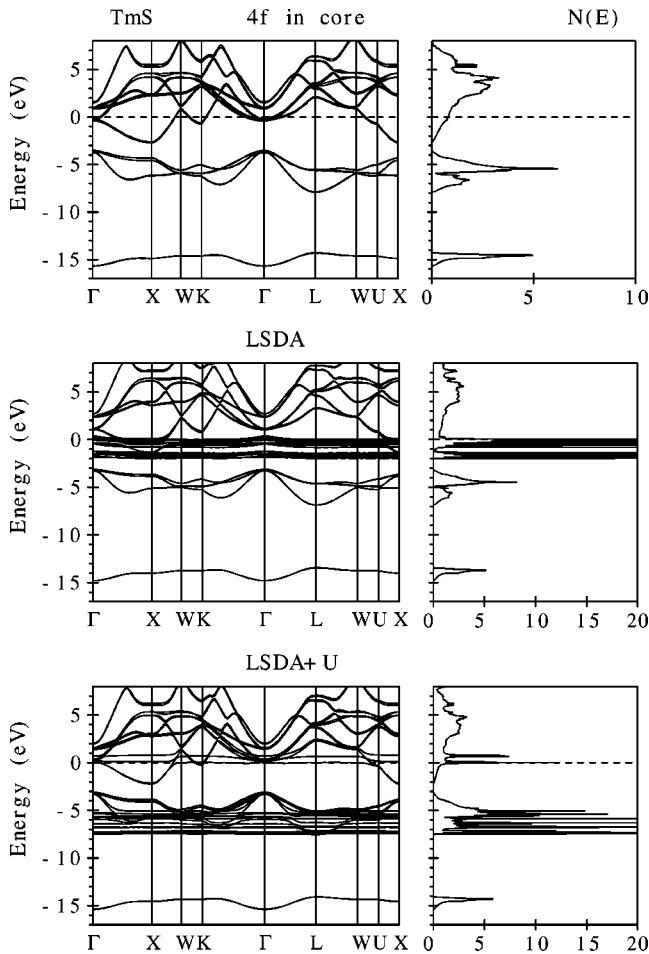


FIG. 1. Self-consistent fully relativistic, spin-polarized energy band structure and total DOS [in states/(unit cell eV)] calculated for TmS treating the $4f$ states as (1) fully localized ($4f$ in core); (2) itinerant (LSDA); and (3) partly localized (LSDA+ U).

structure calculations. We consider the $4f$ electrons as (1) itinerant electrons using the local-spin-density approximation; (2) fully localized, putting them in the core; and (3) partly localized using the LSDA+ U approximation. We note that an important difference with respect to treating the $4f$ electrons as core electrons is that in the LSDA+ U calculation all optical transitions from the $4f$ states are taken into account.

Figure 1 shows the energy band structure of TmS for all three approximations. The energy band structure of TmS with the $4f$ electrons in the core can be subdivided into three regions separated by energy gaps. The bands in the lowest region around -15 eV have mostly S s character with some amount of Tm sp character mixed in. The next six energy bands are S p bands separated from the s bands by an energy gap of about 6.5 eV. The width of the S p band is about 3.7 eV. The spin splitting of the S p bands is very small [about 0.06 eV at the X symmetry point (Fig. 1)]. The highest region can be characterized as Tm spin-split d bands. It is important that the top of the S p bands is at -3.5 eV below the Fermi level since it means that all the interband transitions in the energy interval of 0.0 to 3.5 eV take part within the Tm d bands (see below). The sharp peaks in the DOS

calculated in the LSDA at the Fermi energy and near 2 eV below are due to $4f_{7/2}$ and $4f_{5/2}$ states, respectively (Fig. 1).

In our LSDA+ U band-structure calculations we started from a $4f^{12}$ configuration for the Tm^{3+} ion with twelve on-site $4f$ energies shifted downward by $U_{\text{eff}}/2$ and two levels shifted upwards by this amount. The energies of occupied and unoccupied f levels are separated by approximately U_{eff} . We emphasize, however, that the $4f$ states are not completely localized, but may hybridize, and together with all other states their energy positions relax to self consistency.

The LSDA+ U energy bands and total density of states (DOS) of TmS for $U_{\text{eff}}=6$ eV are shown in Fig. 1. The Coulomb repulsion U_{eff} strongly influences the electronic structure of TmS. For Tm^{3+} ions twelve $4f$ bands are fully occupied and hybridize with S p states. The 14th f hole level is completely unoccupied and well above the Fermi level. A hole 13th f level is pinned at the Fermi level. Although we used a starting configuration with zero occupation of 14th f and 13th f levels, in the process of self-consistent relaxation initially empty 13th f level become partly occupied due to pinning at the Fermi level with occupation number equal to 0.12 (valence 2.88+) in good agreement with the experimental estimations (2.91+) by off-resonance UPS.¹⁴ A fundamental aspect of this observation is that we find the pinning of the 13th f state at E_F to be a robust property of the TmS compound: it happens irrespective of the precise value of U_{eff} .

Photoemission experiments, both x-ray (XPS) and ultraviolet (UPS), have been of central importance for understanding mixed-valence materials (see the review of the early work by Campagna *et al.*)⁹ In rare-earth photoemission, when the photon ejects an electron from the $4f^n$ shell it leaves behind a $4f^{n-1}$ configuration; hence the kinetic energy distribution curve of the emitted electron measures the spectra of the final-state hole. The final state $4f^{n-1}$ has a characteristic multiplet splitting that serves as a fingerprint, and these are accurately resolved and calculable in rare-earth photoemission. By identification of the final-state hole the initial state can be inferred.

The partial $4f$ DOS of the occupied part of the TmS calculated in LSDA and LSDA+ U approximations is compared with UPS measurements¹¹ in Fig. 2. The calculated $4f$ DOS has been broadened to account for lifetime effects and for the experimental resolution. The Tm $4p$ states essentially do not contribute to XPS and UPS because of the low ionization cross section compared with that of the Tm $4f$ states.⁶¹ Hence, the measurements only indicate the f excitation energies of trivalent and divalent Tm, relative to the Fermi level. The LSDA calculations place the $4f$ energy band right at the Fermi level (Fig. 1), producing in the $4f$ DOS a double peak between 0 and -3 eV (Fig. 2). In the LSDA+ U calculations twelve fully occupied $4f$ bands are situated between -4 and -8 eV in the DOS and a partly filled 13th $4f$ band produces a small peak at around -0.5 eV binding energy (Fig. 2).

The LSDA+ U DOS cannot, of course, fully account for the multiplet splitting. Therefore we present at third panel in Fig. 2 the LSDA+ U $4f$ DOS taking into account the multiplet structure of the $4f^{11}$ final state. We used the final-state

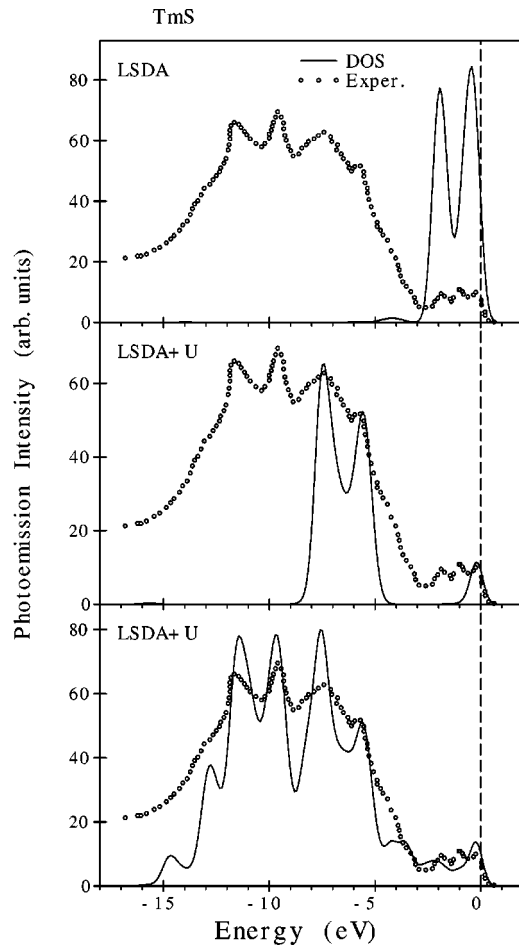


FIG. 2. Comparison the calculated $4f$ DOS in LSDA and LSDA+ U approximations with the experimental UPS spectra from Ref. 14. The third panel from the top shows the LSDA+ U $4f$ DOS taking into account the multiplet structure of the $4f^{11}$ final state (see explanations in the text).

multiplet structure presented in Ref. 9. This multiplet structure consists of 15 terms nine of which are the most intensive ($^4I_{15/2}$, $^4I_{13/2}$, 4F , 2H , 4G , 2K , 4D , 2L , and 2F). The relative intensities for the multiplet peaks were obtained on the basis of calculations⁶² by Cox, who used the fractional parentage method.⁶³ In this method the Hund's rule ground state is assumed for $n4f$ electrons and then the coefficients of fractional parentage (Racah's) for the $n-1$ configurations are calculated. The intensities for the various configurations (multiplets) are just the square of the coefficients of fractional parentage. In the third from the top panel in Fig. 2 the UPS spectrum is modeled by a weighted sum of nine LSDA+ U $4f$ DOS curves. We aligned the centroid of the DOS with each term of the atomic final-state multiplet and summed up the spectra, scaling them according to the relative intensities of the multiplets. The agreement between theory and the UPS measurements is very good. It is clear that the structures between -4.5 and -16 eV binding energy should be assigned to the final-state multiplet structure derived from twelve fully occupied $4f$ bands (Tm^{3+}) and the structures between 0.0 and -4.5 eV are associated with the final-state multiplet structure of the partly occupied 13th f level.

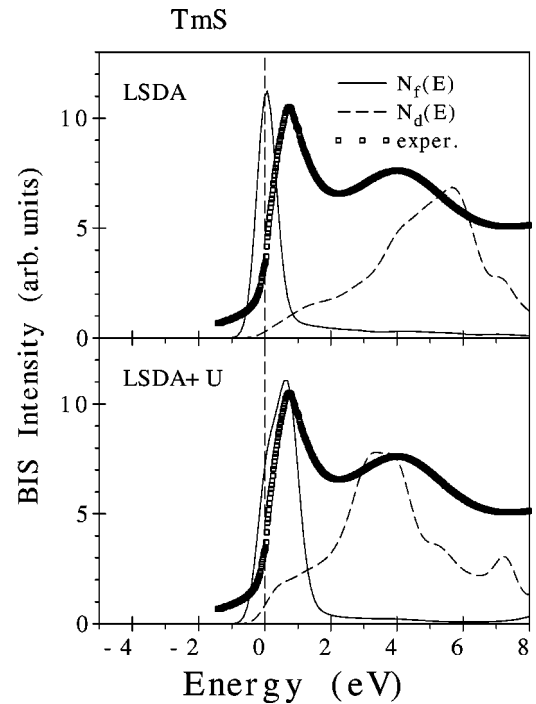


FIG. 3. Comparison of the calculated partial $4f[N_f(E)]$ and $5d[N_d(E)]$ DOS in the LSDA and LSDA+ U approximations with the experimental BIS spectrum of TmS from Ref. 28.

From the good agreement between theory and UPS measurements we may conclude that the LSDA+ U calculations give an accurate position for the occupied $4f$ bands. The principal question is the energy position of the empty $4f$ states, which is usually given by BIS measurements. Figure 3 shows the experimental BIS spectrum²⁸ of TmS compared with the calculated energy distribution for the unoccupied partial $\text{Tm}4f[N_f(E)]$ and $5d[N_d(E)]$ density of states in the LSDA and LSDA+ U approximations. The experimental spectrum consists of two maxima at about 0.9 eV and 4 eV above the Fermi level. The first narrow peak was identified as having f character, whereas the second broad peak was associated with $5d-6s$ states.²⁸ The LSDA places the empty $4f$ states right at the Fermi level, which contradicts the experimental data (Fig. 3). The LSDA+ U calculations place the maximum of the 14th f hole level well above the Fermi level around 0.7 eV. The 13th f hole level is partly occupied with its maximum DOS situated 0.025 eV above the Fermi level (Fig. 1). Due to a rather large experimental resolution of the BIS spectra²⁸ (~ 1 eV) one experimentally observes essentially only a single BIS $4f$ peak instead of two, although a shoulder can be discerned split off from the main peak.²⁸ The LSDA+ U calculations give the correct position of both the $4f$ and $5d$ states (Fig. 3) within the experimental resolution.

More precise information on the band positions may be obtained from optical and MO measurements. Although such measurements have much better resolution (the experimental resolution in optics is always in the meV range) in comparison with XPS and BIS, they produce complex functions containing information of both the initial and final states simultaneously (joint density of states) and are strongly influenced

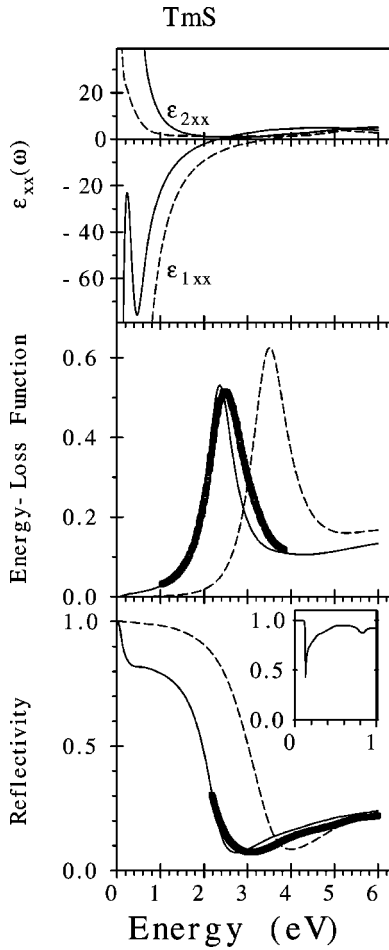


FIG. 4. Calculated real and imaginary parts of the diagonal dielectric function, ϵ_{1xx} and ϵ_{2xx} , energy-loss function, and the optical reflectivity R of TmS treating $4f$ states in core (dashed line) and by the LSDA+ U approximation (solid line) compared with experimental data (solid circles) (Ref. 29).

by the optical transition matrix elements. Besides, the MO spectra strongly depend of the spin and orbital polarization of initial and final states.³³

Figure 4 shows the calculated real and imaginary parts of the dielectric function, $\epsilon_{1xx}(\omega)$ and $\epsilon_{2xx}(\omega)$, the optical reflectivity, and imaginary part of the energy-loss function $\text{Im}[-1/\epsilon(\omega)]$ compared with experimental data.²⁹ We mention, furthermore, that we have convoluted the calculated spectra with a Lorentzian whose width is 0.4 eV to approximate lifetime broadening. On the basis of the results of the LSDA+ U band-structure calculation, the observed optical reflectivity spectrum (Fig. 4) can be sorted into the respective interband transition groups: (1) metallic high reflectivity below ~ 1 eV, (2) a steep edge between ~ 1 and ~ 2.5 eV, and (3) above the minimum at ~ 2.7 eV some less pronounced structures with a broad maximum of R between 5 and 7 eV mostly caused by $3p \rightarrow 5d$ interband transitions.

The predominant structure of the TmS as well as TmSe reflectivity spectra is the edge at 2 eV. This sudden drop is characteristic for metallic rare-earth chalcogenides and is due to a plasma oscillation interfering with interband excitations.²⁹ This plasma resonance causes the golden color

of TmS crystals as it does for all metallic rare-earth sulfides. The energy of the conduction-electron plasma resonance in the presence of the interband excitations is given by $\epsilon_{1xx}(\omega) = 0$. In the particular case of TmS this condition is fulfilled at $\omega = 2.15$ eV and the maximum peak of the energy-loss spectrum in Fig. 4 is shifted only very little from this energy (by -0.05 eV) as a result of damping. The correct energy position of the plasma edge in TmS can be obtained only by taking into account $5d \rightarrow 4f$ interband transitions. The calculations treating $4f$ electrons as core electrons place the zero crossing energy of $\epsilon_{1xx}(\omega)$ at higher energies in comparison with the LSDA+ U calculations and as a result give a wrong energy position for the plasma resonance (Fig. 4).

To search for possible optical $5d \rightarrow 4f$ interband transitions the reflectivity of a TmS single crystal has been measured between 2 meV and 12 eV at room temperature and at 6 K (Ref. 28). One should mention that the observation of optical $5d \rightarrow 4f$ transitions is quite rare, especially when the metal has a large carrier concentration as in the case of TmS with about one carrier per formula unit. The large amount of carriers effectively screens the optical transition as most of the light intensity gets reflected by the plasmons. The chances to observe the optical $5d \rightarrow 4f$ transitions in a metal become only realistic when the energy of the optical transitions is very small since the intensity of the transition scales with ω^{-2} .²⁸ Such a situation occurs in TmS where the partly occupied 13th f hole level is very close to the Fermi level with its maximum DOS situated 25 meV above the Fermi level (Fig. 1). Reflectivity measurements of TmS single crystals in the midinfrared region reveal two lines near 53 and 90 meV.²⁸ The authors interpreted these features as optical transitions from the partly filled $5d$ conduction states near the Fermi level into the empty crystal-field-split 13th band f states (acoustic and optical phonon modes are situated at 13 and 37 meV, respectively, according to Raman scattering measurements.)²⁸ Another less pronounced feature was observed in the reflectivity spectrum measured at 6 K around 0.9 eV. The inset of the Fig. 4 shows the unbroadened theoretically calculated optical reflectivity in the 0 to 1 eV energy interval with two well-pronounced minima at 0.11 and 0.9 eV. These features reflect the interband transitions from occupied $5d$ states to empty 13th f - and 14th f -hole levels situated at 0.025 and 0.7 eV, respectively (Fig. 1). In real optical experiments such transitions are obscured by broadening from intraband Drude-like transitions, lifetime effects, and to a lesser extent the experimental distortion. Figure 5 shows with a logarithmic scale the experimental optical reflectivity spectrum²⁸ of TmS in comparison with the theoretically calculated one. To incorporate the intraband contribution to the optical conductivity tensor we use the phenomenological Drude model⁶⁴ with inverse intraband Drude relaxation time $\gamma_D = 0.1$ eV. We also take into account a lifetime broadening with a Lorentzian width of 0.1 eV.

The position of the second less-pronounced minimum arising from the $5d$ to 14th f interband transitions is in good agreement with the experimental measurements (Fig. 5). We have not included in our band-structure calculation the crystal-field effects, so we obtained a single feature in the

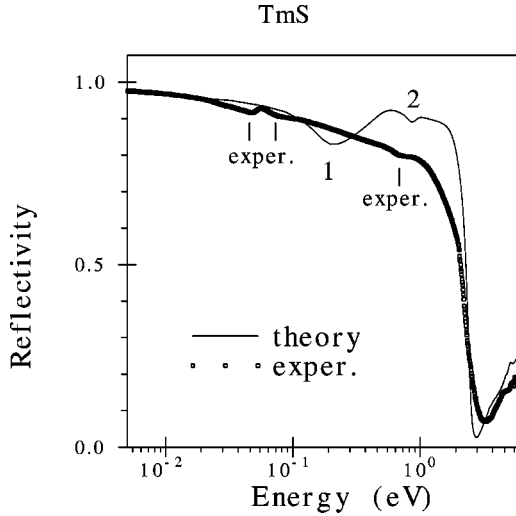


FIG. 5. Calculated optical reflectivity spectrum of TmS compared with experimental data (Ref. 28).

optical reflectivity at 110 meV instead of two experimentally measured features at 53 and 90 meV due to crystal-field splitting.²⁸ The small shift of the theoretically calculated feature towards larger photon energies in comparison with the optical measurements may be due to a valence-band electron-hole interaction in the optical spectrum that is absent in photoemission or BIS experiments as well as in our one-particle LSDA+ U calculations. We should mention that the incorporation of the electron-hole excitations in the band-structure calculations is a nontrivial task and requires an effective two-body approach (see Ref. 65 and references therein). It is beyond our capacity now.

After consideration of the band structure and optical properties we turn to the magneto-optical spectra. In the polar geometry, where the z axis is chosen to be perpendicular to the solid surface, and parallel to the magnetization direction, the expression for the Kerr angle can be obtained easily for small angles and is given by³³

$$\theta_K(\omega) + i\varepsilon_K(\omega) = -\sigma_{xy}(\omega)/D(\omega), \quad (2)$$

$$D(\omega) = \sigma_{xx}(\omega) \sqrt{1 + \frac{4\pi i}{\omega} \sigma_{xx}(\omega)}, \quad (3)$$

with θ_K the Kerr rotation and ε_K the so-called Kerr ellipticity. $\sigma_{\alpha\beta}$ ($\alpha, \beta \equiv x, y, z$) is the optical conductivity tensor, which is related to the dielectric tensor $\varepsilon_{\alpha\beta}$ through

$$\varepsilon_{\alpha\beta}(\omega) = \delta_{\alpha\beta} + \frac{4\pi i}{\omega} \sigma_{\alpha\beta}(\omega). \quad (4)$$

In Fig. 6 we show the experimental³¹ $\theta_K(\omega)$ and $\varepsilon_K(\omega)$ MO Kerr spectra of TmS, as well as the spectra calculated with LSDA and LSDA+ U , and with the $4f$ electrons in the core. This picture clearly demonstrates that the better description is unambiguously given by the LSDA+ U approach. The most prominent discrepancy in the LSDA spectra is the extra peaks between 0 and 2 eV caused by interband transitions involving the hybridized $4f$ states,

which in the LSDA approach exhibit a maximum resonance near E_F . In the LSDA+ U approach, the occupied $4f$ state energies are shifted downward due to the on-site Coulomb interaction U_{eff} . As a result, the transitions involving the occupied $4f$ states do not take place at small photon energies, and the erroneous peak structures around 0 to 2 eV disappears from the Kerr spectra. The calculations in which the $4f$ electrons are treated as quasicore are able to reproduce structure similar to the LSDA+ U calculations, but in wrong the positions. Besides, due to the lack of corresponding $5d \rightarrow 4f$ interband transitions, the off-diagonal part of the optical conductivity $\sigma_{2,xy}$ is nearly zero, so that a very small Kerr rotation is obtained.

Off-diagonal optical conductivity of TmS shows very large values at low energies with a marked extremum in $\sigma_{2,xy}(\omega)$ near 0.5 eV and it is almost constant in the 2 to 4 eV energy interval (Fig. 6). As a result the shape of the Kerr ellipticity and Kerr rotation spectra in this compound are completely determined by a shape of the function $[\omega D(\omega)]^{-1}$ in Eq. (2).

The situation is clearly seen in Fig. 7, where we show the theoretically calculated Kerr rotation and ellipticity of TmS using the LSDA+ U approximation and the frequency dependence of real and imaginary parts of the function $[\omega D(\omega)]^{-1}$ multiplied by a constant to normalize the spectra. Obviously the shape of the Kerr spectra in TmS results mostly from the resonance structure of the function $[\omega D(\omega)]^{-1}$. Actually our first-principles band-structure calculations confirm the idea already drawn by Feil and Haas in Ref. 66 on the basis of model calculations that the sharp Kerr effect in some magnetic metallic rare-earth compounds including TmS and TmSe is not due to the electronic interband transitions, but rather to the influence of a plasma resonance.

B. TmTe

Figure 8 shows the energy band structure and total density of states of TmTe calculated in LSDA and LSDA+ U approximations. Although TmTe is known as a magnetic semiconductor, LSDA calculations gave a metallic solution.

In contrast to LSDA, the LSDA+ U calculations predicts a correct ground state of TmTe, namely, a magnetic semiconductor with direct energy gap of 0.86 eV at the Γ symmetry point and an indirect gap of 0.58 eV between the top of Tm $4f$ valence band at the Γ point and the bottom of Tm $5d$ conduction band at the X symmetry point. Theory produces a somewhat larger energy gap in comparison with the optical measurements of 0.35 eV.² Thirteen completely occupied Tm $4f$ energy bands located between 0.0 and -2.2 eV are hybridized with Te $5p$ states. The empty 14th f energy level is situated around ~ 5.8 eV above the Fermi level hybridized with Tm $5d$ states (Fig. 8). In other words, theory predicts the Tm atom in TmTe to be in divalent state.

The most striking evidence for the absence of any mixed valence state in TmTe comes from photoemission measurements. It was shown in the Ref. 2 that the amount of detectable Tm^{3+} in UPS measurements depends strongly on the surface condition, and that the ratio of $\text{Tm}^{3+}/\text{Tm}^{2+}$ increases after cleavage as a function of time from a value $\leq 6\%$. Also,

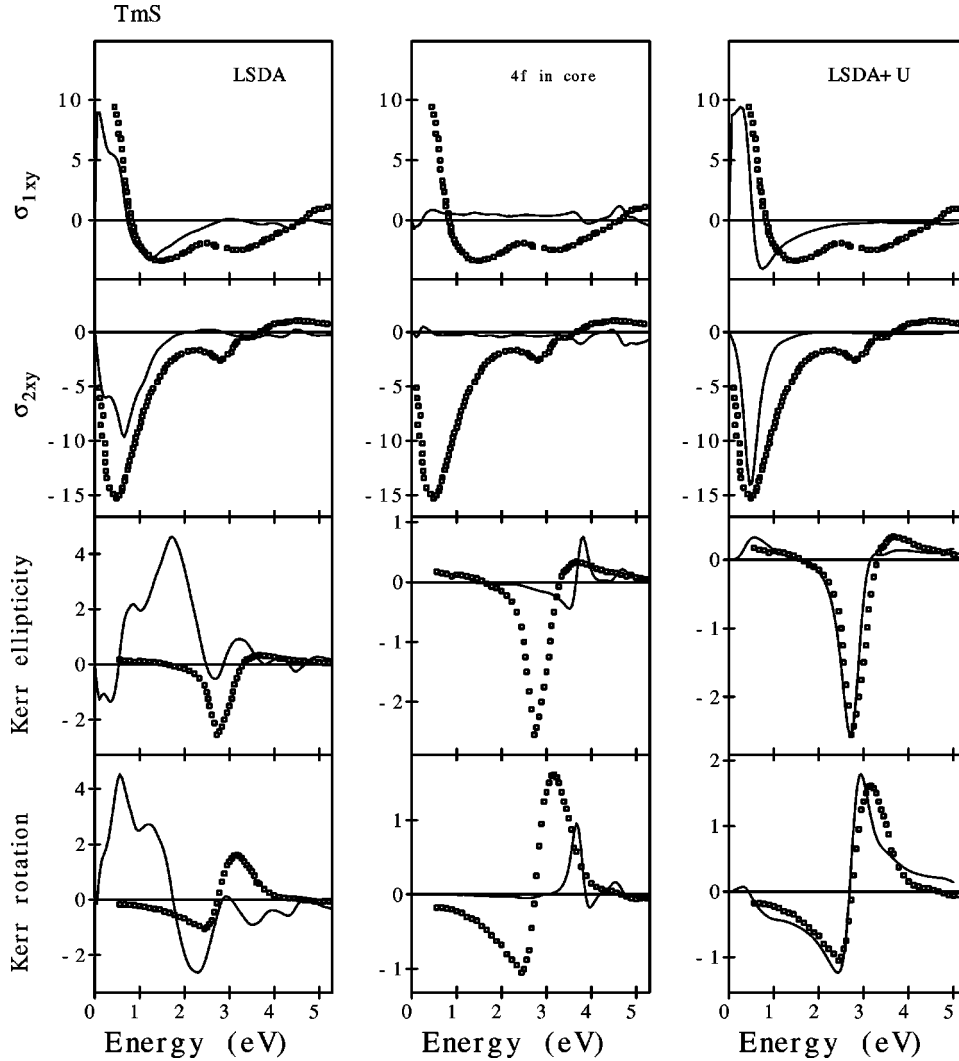


FIG. 6. Calculated off-diagonal parts of the dielectric function ϵ_{xy} (in 10^{29} s^{-2}), Kerr rotation and Kerr ellipticity spectra (in degrees) for TmS treating the $4f$ states as a core electrons, and LSDA and LSDA+ U approximations compared with experimental data (circles) (Ref. 31).

the absorption spectrum of vacuum-cleaved TmTe, as derived from the reflectance, shows clear evidence for transitions from Tm^{2+} in the energy region 0 to 7 eV, but no conclusive indication of transitions from Tm^{3+} in the energy region 7 to 14 eV.²

A recent more precise photoemission study of TmTe (Ref. 14) gives the mean valence value equal to 2.15+ and 2.35+ from the study of the total yield and off-resonance photoemission spectra, respectively, although the mean valence of the same sample obtained from the result of magnetic susceptibility measurement is 2.017+. The valency of the Tm ion in TmTe from lattice constant considerations was found to be 2.0+.¹ Thus it would seem that the trivalent component observed in photoemission measurements mainly comes from the surface. Besides, the valence structure of such samples strongly depends on the stoichiometry. Figure 9 shows TmTe UPS spectrum¹⁴ in comparison with the occupied part of the partial LSDA+ U $4f$ DOS calculated with a multiplet structure of $4f^{12}$ final state taken into account in the same way as for TmS. The multiplet structure consisting of six terms (3H , 3F , 3P , 1I , 1G , 1D , and 1S) was taken from Ref. 9. We conclude that the structures between 0.0 and -8 eV binding energy is associated with the $4f^{12}$ final-state

multiplet structure. The structures with higher binding energies should be assigned to the final-state $4f^{11}$ multiplet structure of the Tm^{3+} ions mainly coming from the surface. To check this we calculated the energy band structure and $4f$ DOS of TmTe using a starting configuration with zero occupation of the 14th f and 13th f levels (Tm^{3+} configuration) and we took into account a multiplet structure of the $4f^{11}$ final state.⁹ As seen from Fig. 9 the $4f^{11}$ final-state multiplet structure corresponds to structures seen in the -4 to -16 eV energy interval. Hence, the contribution to the peaks at around -5.5 and -7.5 eV binding energy in UPS measurements come from both the Tm^{2+} and Tm^{3+} ions. Besides, there are also contributions to the main feature of the UPS spectrum at 0 to -3 eV binding energies coming from the partly filled 13th f level of the Tm^{3+} ions.

The pressure effects on transport properties of TmTe were investigated by Matsumura *et al.*²⁵ It was found that at room temperature, the resistivity of TmTe showed an exponential decrease up to 2 GPa, indicating a linear closing of the energy gap (with $d\Delta/dP = -207 \text{ meV/GPa}$), followed by an almost pressure-independent metallic regime. In order to investigate the influence of pressure on the electronic structure of TmTe we performed self-consistent energy band-structure

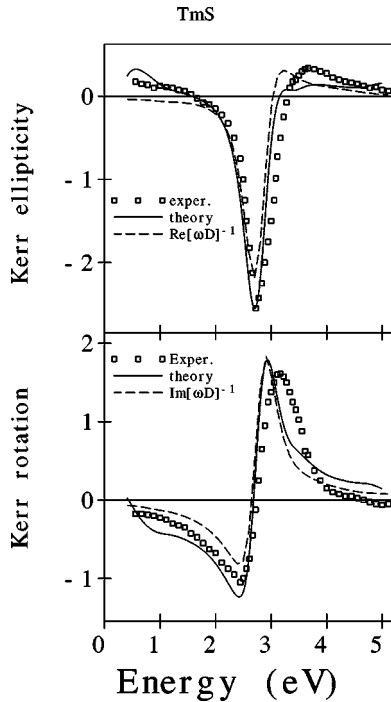


FIG. 7. Calculated Kerr rotation and Kerr ellipticity spectra (in degrees) for TmS in the LSDA+ U approximation, and real and the imaginary parts of the function $[\omega D(\omega)]^{-1}$ compared with experimental data (Ref. 31).

calculations for several reduced lattice constants. We found a gradual decreasing of the energy gap and closing of the indirect gap at $a=6.05$ Å in a good agreement with experiment. The semiconductor-metal phase transition for pure TmTe takes place at around ~ 2.5 GPa.²⁵ The *composition-*

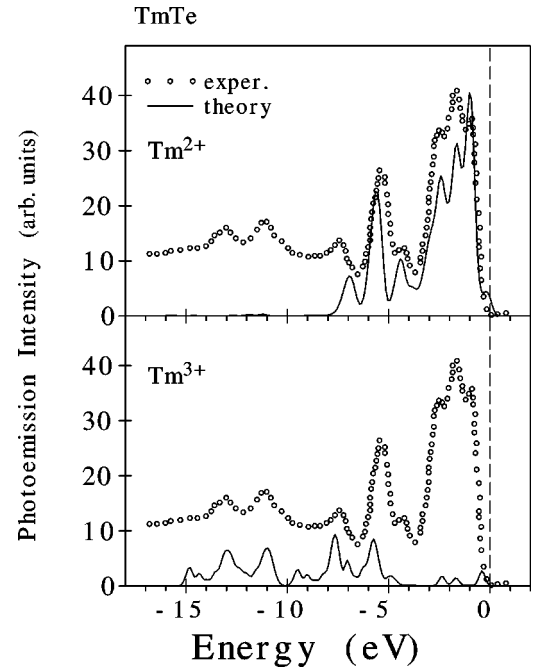


FIG. 9. Comparison of the calculated Tm²⁺ and Tm³⁺ 4f DOS of TmTe in LSDA+ U approximation, taking into account the multiplet structure of 4f¹² and 4f¹¹ final states with the experimental UPS spectra from Ref. 14.

ally induced semiconductor-metal transition in the TmSe_{1-x}Te_x system takes place for $x=0.4$ with the lattice constant³ equal to ~ 6.02 Å (Ref. 3) (see below).

There is no experimental measurements of the MO spectra for TmTe. The measurements have been performed only for the TmSe_{0.32}Te_{0.68} system.³³ The theoretical analysis of the MO spectra of TmSe_{0.32}Te_{0.68} will be considered below.

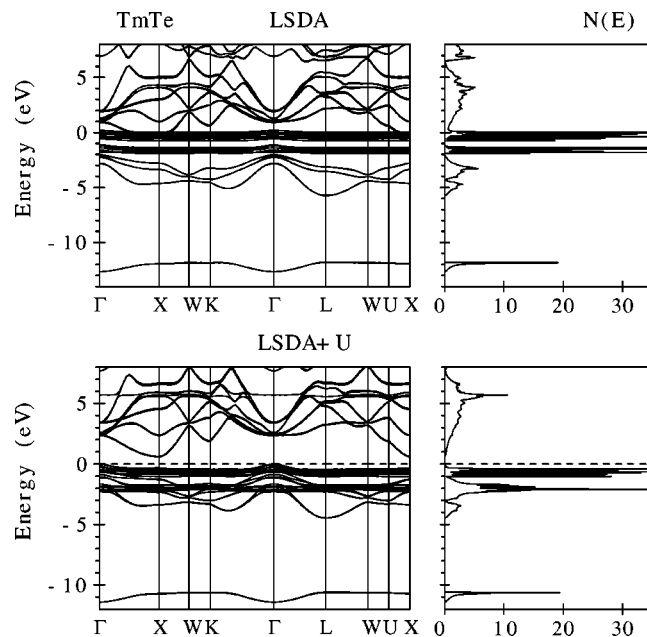


FIG. 8. Self-consistent fully relativistic, spin-polarized energy band structure and total DOS (in states/(unit cell eV)) calculated for TmTe.

C. TmSe

The simplest argument that TmS is trivalent, TmSe intermediate valent, and TmTe divalent under normal conditions comes from comparing the lattice constants of rare-earth sulfides, selenides, and tellurides as done by Bucher *et al.*¹ The lanthanide contraction is the cause for the general trend in the curves, and the standard divalent Sm, Eu, and Yb ions with their larger ionic radius are the obvious deviations. TmTe lies on the divalent curve, TmS on the trivalent one, and TmSe is intermediate, and by linear interpolation between a hypothetical divalent and trivalent TmSe one obtains a valence of Tm^{2.75+}. Further evidence that TmSe is intermediate valence comes from x-ray and ultraviolet photoemission spectroscopy measurements.^{9,14} The photoemission study¹⁴ of TmSe gives the mean valence value equal to 2.79 and 2.68 from study of the total yield spectra and off-resonance photoemission respectively, although the mean valence of the same sample obtained from magnetic susceptibility measurement is 2.53. We should mention that the total yield spectra reflect more bulk information than photoemission spectra and the values obtained from transport properties or magnetic susceptibility are mostly bulk and not surface sensitive.¹⁴

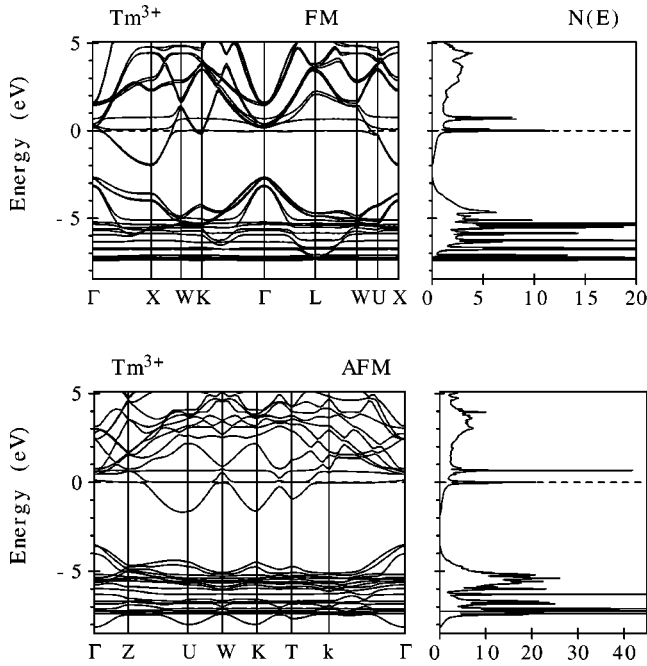


FIG. 10. Self-consistent fully relativistic, spin-polarized energy band structure and total DOS [in states/(unit cell eV)] calculated for TmSe in ferromagnetic (FM) and antiferromagnetic (AFM) ordering.

The ground state of an intermediate-valence compound is a quantum mechanical mixture of both the $4f^n$ and the $4f^{n-1}5d$ configuration on each rare-earth ion. Such compounds need theoretical consideration beyond the mean-field one-particle LSDA+ U approximation due to possible configuration interaction between different $4f$ valence states. Although such interactions should be less in Tm compounds in comparison, for example, with mixed-valent Ce compounds due to contraction of the $4f$ wave function, it can lead to a spontaneous interconfiguration fluctuations (ICF), introduced first by Hirst.⁶⁷ As briefly discussed by Varma,⁶⁸ at $T=0$, fluctuations could be either static or dynamic. In the static case the system is spatially “inhomogeneous” in the sense that at inequivalent sites different valence states are present. Examples among the rare-earth compound are Eu_3S_4 or Eu_3O_4 .⁹ Such static charge “fluctuations” have been known for a long time in the $3d$ series, Fe_3O_4 , magnetite, being a typical example (see Ref. 39 and references therein). In the dynamic case the system shows fast local fluctuations which give an intrinsic width to the f levels. At any given site $4f$ charge fluctuations between the two configurations occur on a time scale τ_{ICF} , the so called *interconfiguration fluctuation time*. The system on time average is “homogeneous,” i.e., all sites are equivalent. TmSe is known to be a homogeneous mixed-valence compound.⁹ Experiments such as lattice constant and isomer shift measurements, which probe the sample on a time scale much longer than τ_{ICF} , will “see” only one intermediate configuration, but experiments such as XPS or UPS measurements, which take place in a time much shorter than τ_{ICF} (up to 10^6 – 10^7 times shorter)¹⁰ will “see” the instantaneous picture of a mixture of the ions in the two valence states.

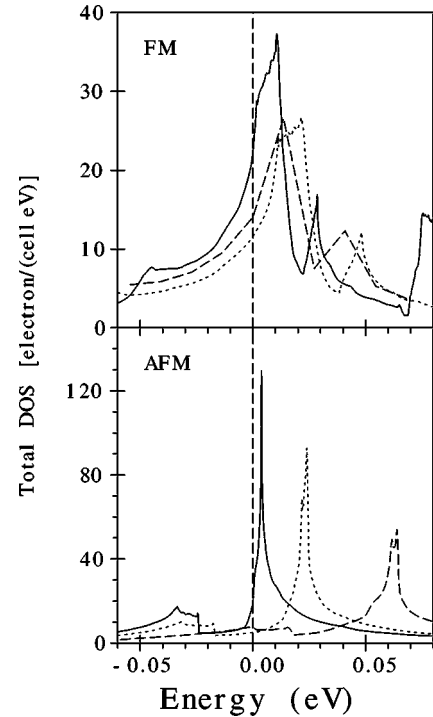


FIG. 11. Expanded view of the DOS of TmSe (solid line), TmS (dotted line), and TmSe with the lattice constant of TmS (dashed line) calculated in the LSDA+ U approximation for ferromagnetic (FM) and antiferromagnetic (AFM) ordering.

The LSDA+ U energy bands and total density of states of TmSe for $U_{\text{eff}}=6$ eV are shown in Fig. 10 both for the ferromagnetic and antiferromagnetic ordering for the Tm^{3+} ions. Our band-structure calculations gave for the fcc type-II antiferromagnetic phase lower total energy in comparison with fcc type-I phase. We have verified, however, that neither the Tm magnetic moment nor spectral properties depend strongly on the type of antiferromagnetic order. For example, the difference in the magnetic moments is about $0.01\mu_B$. Therefore, we present only the results for the fcc type-II antiferromagnetic phase of TmSe. The electronic structure of TmSe for the Tm^{3+} ions is very similar to the TmS one with twelve $4f$ bands fully occupied and hybridized with chalcogenide p states. The 14th f hole level is completely unoccupied and well above the Fermi level. A hole 13th f level is partly occupied and pinned at the Fermi level. The occupation number of the 13th f level is equal to 0.27 (valence 2.73+) in good agreement with estimations from the lattice constants (2.75+) as done by Bucher *et al.*¹ and from UPS measurements (2.79+ and 2.68+ from total yield and photoemission spectra respectively).¹⁴

Figure 11 shows the expanded view of the total DOS of TmSe and TmS both in the ferromagnetic (FM) and antiferromagnetic (AFM) states. An important feature of the FM electronic structure is a high DOS at the Fermi energy E_F in both TmS and TmSe. A large DOS at E_F signals an instability with respect to metamagnetic phase transitions. Indeed, total energy calculations show that the ground state for TmSe as well as for TmS is an antiferromagnetic ordering in agreement with experiment.^{8,18} Through the FM-AFM phase tran-

sition a pseudogap at the Fermi level is opened in both TmS and TmSe (Fig. 11). The opening of such a pseudogap may explain the increasing of the electrical resistivity below the Néel temperature,^{18,20,21} as well as an enormous negative magnetoresistivity associated with the metamagnetic transition to the high-field aligned state and decreasing of the Hall coefficient in an external magnetic field.²²

The pinning of a partly occupied 13th f level is different in TmS and TmSe. In contrast to TmS, the Fermi level crosses the 13th f hole level in the vicinity of its DOS maximum in TmSe, both in the FM and the AFM states. The maximum DOS of the 13th f hole level is situated above the Fermi level, as close as 4 meV (~ 45 K) in the AFM ground state of TmSe. The energy position of the 13th f level is in a good agreement with low temperature far-infrared optical measurements by Marabelli and Wachter.⁶⁹ According to their measurements the first interband transition appears at about 3 meV. We should mention here that when we speak about partial occupation of the 13th f hole level in TmS we mean that such an occupation is due to the hybridization effect between $5d$ and $4f$ energy states. The peak position of the 13th f hole level DOS in TmS is relatively far away from the Fermi level. A different situation occurs in TmSe where the Fermi level crosses the shoulder of the 13th f -hole level DOS (see Fig. 11); hence the 13th f level is really pinned at the Fermi level. It is a typical situation for mixed-valent crystals.

The Tm monochalcogenides offer the unique opportunity to follow the evolution of intermediate valence as a function of composition. The driving force is the change of lattice constant upon exchanging the anion. In order to separate the influence of the lattice constant from the influence of the ionic potential of the chalcogenide component on the electronic structure of TmX ($X = S$ and Se), we present in Fig. 11 also the DOS of TmSe evaluated with the lattice constant of TmS. The partial occupation of the 13th hole f level in this case is similar to the situation for TmS, although the energy positions of the maxima are not the same as in actual TmS. The mean valency of TmSe with the lattice constant of TmS is equal to 2.90+, very close to valency in actual TmS (2.88+). It can be considered as qualitative theoretical support of the conclusion derived in Ref. 24 that the application of pressure enhances the Tm^{3+} state relative to Tm^{2+} state in the TmSe.

In Fig. 12 the partial $4f$ DOS of the occupied part of the TmSe band structure is compared with XPS measurements⁹ for two single crystals with different lattice constants. An off-stoichiometric violet TmSe single crystal, with lattice constant $a = 5.640 \text{ \AA}$, contains almost entirely Tm^{3+} ions.⁹ The theory calculations using a starting configuration with zero occupation of 14th f and 13th f levels (Tm^{3+} configuration) well describe this experimental XPS spectrum.

The XPS spectrum of TmSe with $a = 5.689 \text{ \AA}$ has a sizeable divalent signal between 0 and -3 eV binding energy. The second panel from the top of Fig. 12 shows the theoretically calculated $4f$ DOS of the Tm^{2+} Se, taking into account the multiplet structure of the $4f^{12}$ final state. The last panel shows the experimental XPS spectrum for $a = 5.689 \text{ \AA}$ in comparison with the sum of Tm^{3+} and Tm^{2+} $4f$ DOS's in a

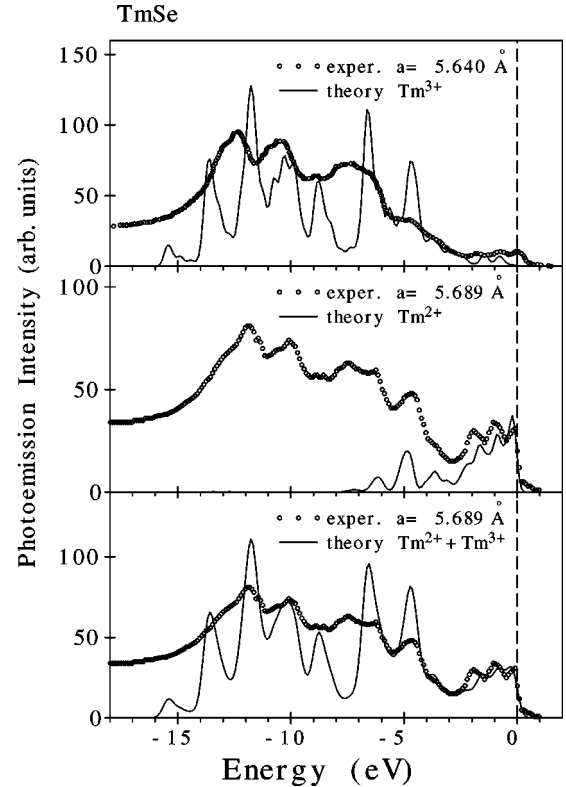


FIG. 12. The calculated Tm^{3+} and Tm^{2+} $4f$ DOS of TmSe in LSDA+ U approximations, taking into account the multiplet structure of the $4f^{12}$ and $4f^{11}$ final states. Comparison is made with the experimental XPS spectra from Ref. 9 measured for two different lattice constants.

50-50 proportion. These results suggest that the valency of the sample with $a = 5.689 \text{ \AA}$ is close to 2.5 which comes from the analysis of the DOS's. Of course it is difficult to make quantitative conclusions about the possible $Tm4f$ configuration in TmSe from comparison of theoretically calculated $4f$ DOS with XPS or UPS spectra. From such a comparison we can only derive an energy position of final-state multiplet structures from Tm^{3+} and Tm^{2+} ions. The XPS and UPS spectra are strongly affected by the transition matrix elements, which we omitted in our consideration for simplicity. Besides, the relative intensities of Tm^{3+} and Tm^{2+} ion final-state multiplet structures depend on the excitation photon energy. This was shown in Ref. 14 where the intensity ratio between the trivalent and divalent components in Tm monochalcogenides change significantly depending on resonance or off-resonance conditions. Finally, UPS and XPS spectroscopies are strongly surface-sensitive methods. The escape depth of a photoelectron with kinetic energy of a kilovolt is about 15 Å. For the softer radiation typical for the UPS measurements (≤ 100 eV) the escape depth is only about 4 Å,⁷ hence only the surface layers are probed. A recent advance in our understanding of mixed-valent photoemission comes from the recognition that surface spectra can be markedly different from that of the bulk. In particular the valence at the surface can be very different.⁷

In the optical reflectivity measurements the depth of penetration is given by the inverse absorption coefficient and

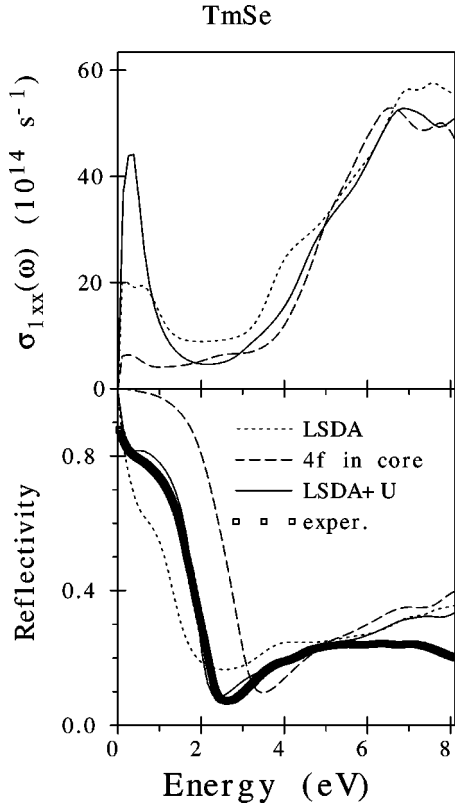


FIG. 13. Calculated diagonal part of the optical conductivity σ_{1xx} and the optical reflectivity R of TmSe treating the $4f$ states as (1) fully localized ($4f$ in core) (dashed line); (2) itinerant (LSDA) (dotted line); and (3) partly localized (LSDA+ U) (solid line) compared with the experimental data (Ref. 29) (open squares).

typically amounts to 10^2 to 10^3 Å. This means that the optical and MO measurements are not so surface sensitive.

Figure 13 shows the calculated diagonal part of the optical conductivity σ_{1xx} and the optical reflectivity of TmSe treating the $4f$ states as (1) fully localized ($4f$ in core); (2) itinerant (LSDA); and (3) partly localized (LSDA+ U) in comparison with experimental data.²⁹ The calculations treating $4f$ electrons as core electrons place the zero crossing energy of $\epsilon_{1xx}(\omega)$ at higher energies in comparison with the LSDA+ U calculations and as a result give a wrong energy position for the plasma resonance, which determines a deep minimum in the optical reflectivity (Fig. 13). Due to the wrong position of $4f$ energy bands in the LSDA calculations this approximation is not able to produce the correct optical reflectivity in the infrared spectral region. Figure 13 clearly demonstrates that the better description of the optical reflectivity spectrum is given by the LSDA+ U approach. The $5d \rightarrow 4f$ interband transitions play an essential role in the fast decrease of the optical reflectivity in 0 to 0.5 eV energy interval.

In Fig. 14 we show the experimental³² $\theta_K(\omega)$ and $\epsilon_K(\omega)$ MO Kerr spectra of TmSe, as well as the spectra calculated with LSDA and LSDA+ U . The better description is unambiguously given by the LSDA+ U approach. The most prominent discrepancy in the LSDA Kerr spectra is the extra peak at 0.5 eV, which is caused by extra structure present in

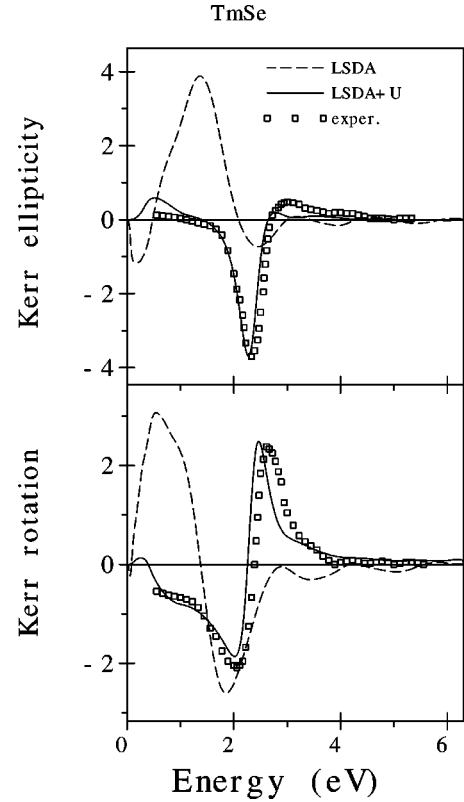


FIG. 14. Calculated Kerr rotation and Kerr ellipticity spectra (in degrees) for TmSe in the LSDA (dashed line) and LSDA+ U (full line) approximations compared with experimental data (open squares) (Ref. 32).

the dielectric tensor. Responsible are interband transitions involving the hybridized $4f$ states, which in the LSDA approach exhibit a maximum resonance near E_F . In the LSDA+ U approach, the occupied $4f$ state energies are shifted downward due to the on-site Coulomb interaction U_{eff} . As a result, the transitions involving the occupied $4f$ states do not take place at small photon energies, and the erroneous peak structure around 0.5 eV disappears from Kerr spectra.

Some experimental results^{3,26,69,70} indicate that TmSe could be a narrow-gap semiconductor below the Néel temperature. Evidence for a hybridization gap comes from the activated behavior of the electrical resistivity⁷ and from a large negative value of the Hall coefficient at 3.5 K,⁷ suggesting fewer than 10^{18} carriers per cm^3 . Other evidence that stoichiometric TmSe might be a narrow-gap semiconductor comes from point-contact measurements.²⁶ The dynamic resistance $dV/dI(V)$, which for intermediate-valence materials is proportional to $1/N(E)$ has a peak at E_F in the AFM state. Such a peak disappears in an external magnetic field above 10 kOe where TmSe exhibits a ferromagnetic order. A maximum in $dV/dI(V)$ corresponds to a minimum in $N(E)$ —a gap or at least a pseudogap. The estimations from the activation energy in electrical resistivity measurements and from point-contact spectra shows a possible gap of about 1 to 2 meV.³

On the other hand, some experiments indicate that there may not be a gap but rather a pseudogap, and the hybridization does not occur over whole Brillouin zone. The electrical resistivity is raised only about one order of magnitude through the FM→AFM phase transition.³ Direct optical measurements by Batlogg *et al.*⁷¹ show a metallic reflectivity in Tm_{1-x}Se with a reflectivity edge that shifts about 0.5 eV as x varies from thulium deficiency to excess. Such studies as a function of stoichiometry give convincing evidence that the intrinsic TmSe behavior is metallic. More recent optical measurements by Marabelli and Wachter⁶⁹ show that during the measurements they always found a free carrier behavior for the lowest energies, then a gap or a pseudogap followed by a first interband transition at about 3 meV.

In our LSDA+ U band-structure calculations of TmSe we used a starting configuration with zero occupation of 14th and 13th f levels. In the process of self-consistent relaxation the 14th f -hole level is situated well above the Fermi level, but the initially empty hole 13th f level becomes partly occupied due to pinning at the Fermi level with occupation number equal to 0.27 (valence 2.73+) producing a metallic AFM ordered ground state with a pseudogap at the Fermi level. Such an energy band structure describes the energy distribution curve of the UPS spectrum well, in addition to the optical and MO spectra of TmSe (see Figs. 12, 13, and 14, respectively). We should mention that the more sophisticated LDA++ method,³⁵ which takes into account the energy dependence of the electron self-energy, also failed to obtain an insulating AFM ground state in TmSe. The possible appearance of such an energy gap in TmSe might be caused by both hybridization and exciton effects due to the Coulomb attraction of the $5d$ conduction electron and $4f$ hole.³⁵ This effect is not described in the LSDA+ U and LDA++ methods. This mechanism requires further theoretical investigations. Additional experimental low-temperature optical ir measurements on good-quality single crystals of TmSe are highly desired.

D. $\text{TmSe}_{1-x}\text{Te}_x$ system

The alloy system $\text{TmSe}_{1-x}\text{Te}_x$ is one of the most important alloy systems in the field of intermediate valence since it keeps the important cation untouched while exhibiting intermediate-valent metals, intermediate-valent semiconductors, semiconductor-metal transitions, ferro- and antiferromagnets and a new ground state of condensed matter, the excitonic insulator.³ The study of the physical properties of the $\text{TmSe}_{1-x}\text{Te}_x$ system offers an interesting possibility to go from integer divalent semiconducting $\text{TmTe}(x=1)$ to intermediate-valent metallic $\text{TmSe}(x=0)$. The substitution of Te by smaller Se ions causes a reduction of the lattice constant. The reduction of the lattice spacing for the Tm ions due to the substitution is often termed *chemical pressure*. The system $\text{TmSe}_{1-x}\text{Te}_x$ shows a *compositionally induced* semiconductor-metal transition.⁷² For $x > 0.4$ the compounds are semiconducting and for $x < 0.18$ metallic. Both phases are separated by a miscibility gap. The substitution of Te by Se reduces the energy gap, resulting in a decrease of the

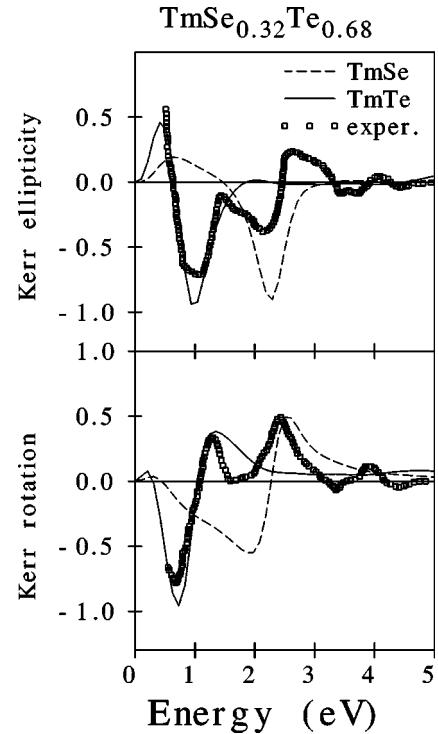


FIG. 15. The experimental (open squares) Kerr rotation and Kerr ellipticity spectra (in degrees) for $\text{TmSe}_{0.32}\text{Te}_{0.68}$ (Ref. 33) in comparison with LSDA+ U calculated spectra for TmSe and TmTe with a proportion of 32% and 68%, respectively.

electrical resistivity and an increase of the electron concentration by about three orders of magnitude.⁷²

There are two major effects occurring in the process of substitution: reduction of the lattice constant and increase of Tm valency. There is also a clear deviation from the Vegard-law (linearity between lattice constant and valence) line for divalent Tm with increasing substitution of Se ions. As for x in the range of 0 to 0.18 the Tm valency is within the 2.9 to 2.8 interval, and for $0.4 \leq x \leq 1.0$ the valency is in the interval of 2.3 to 2.0.

The experimental measurements of MO spectra for $\text{TmSe}_{0.32}\text{Te}_{0.68}$ have been presented in Ref. 33. This particular compound has a lattice constant equal to 6.21 Å and a Tm valency of about 2.08+.⁷² The compound is a mixture of Tm^{2+} and Tm^{3+} ions. Figure 15 shows the theoretically calculated Kerr rotation and Kerr ellipticity spectra of TmSe and TmTe compounds with the intensity of the spectra scaled in the proportion of 0.32 and 0.68, respectively, to make comparison with the experimental $\text{TmSe}_{0.32}\text{Te}_{0.68}$ spectra. We used the lattice constant of 6.21 Å for both the TmSe and TmTe compounds. It can be seen from Fig. 15 that the deep negative minimum at 0.7 eV and positive peak at 1.2 eV in the Kerr rotation spectrum of $\text{TmSe}_{0.32}\text{Te}_{0.68}$ are mostly determined by the divalent Tm ions, and the rest of the fine structure of the Kerr spectrum is derived from interband transitions involved the Tm^{3+} ions.

E. $\text{Tm}_{1-x}\text{Eu}_x\text{Se}$ and $\text{Tm}_{1-x}\text{Y}_x\text{Se}$ systems

Another possibility to investigate the electronic structure of thulium monochalcogenides comes from partial substituti-

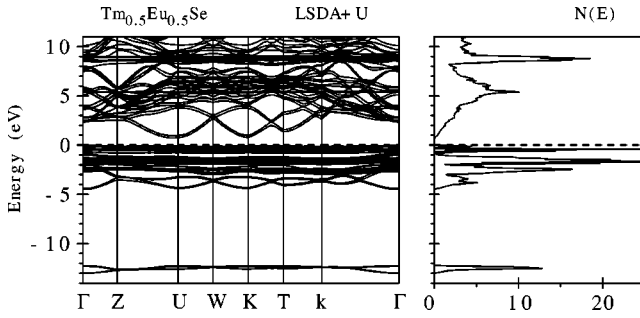


FIG. 16. Self-consistent LSDA+ U fully relativistic, spin-polarized energy band structure and total DOS [in states/(unit cell eV)] calculated for $\text{Tm}_{0.5}\text{Eu}_{0.5}\text{Se}$.

tion of Tm ions by divalent Eu^{2+} ions or trivalent Y^{3+} ions. Let us consider both situations. In the $\text{Tm}_{1-x}\text{Eu}_x\text{Se}$ pseudobinary alloy system the substitution of Tm by Eu increases the lattice constant since divalent Eu has a larger ionic radius than divalent Tm. Kaldis *et al.*⁷³ have shown that for $x = 0.2$ a compositionally induced metal-semiconductor transition is found, i.e., for $x > 0.2$ the compounds become semiconductors. A number of miscibility gaps exist in a small concentration range above $x = 0.2$. Tm as well as Eu remains divalent for $x > 0.2$.

To study the effect of Eu and Y substitution we performed self-consistent band-structure calculations for a supercell containing two formula units that corresponds to $\text{Tm}_{0.5}\text{Eu}_{0.5}\text{Se}$ and $\text{Tm}_{0.5}\text{Y}_{0.5}\text{Se}$ compositions. Figure 16 shows the energy band structure and total density of states of $\text{Tm}_{0.5}\text{Eu}_{0.5}\text{Se}$ calculated in the LSDA+ U approximation. In contrast to LSDA, which gave a metallic solution (not shown), the LSDA+ U calculations for the Tm^{2+} and Eu^{2+} ions predict a correct ground state of $\text{Tm}_{0.5}\text{Eu}_{0.5}\text{Se}$, namely, a ferrimagnetically ordered semiconductor with a direct energy gap of 0.65 eV at the Γ symmetry point and an indirect energy gap of 0.57 eV between the top of the Tm4*f* valence band at the Γ point and the bottom of the Tm5*d* conduction band at the K point. As in the case of pure TmTe, the theory gives a larger energy gap in comparison with the optically measured value of 0.1 eV (for $\text{Tm}_{0.6}\text{Eu}_{0.4}\text{Se}$ compound). The bands in the lowest region around -13 to -12 eV have mostly Se *s* character. The Se *p* bands separated from the *s* bands by an energy gap of about 7.5 eV are located between -4.5 to -1.7 eV. Thirteen completely occupied Tm4*f* energy bands are situated in the 0.0 to -2.0 eV energy interval hybridized with Se5*p* states. Seven occupied Eu4*f* energy bands are situated in the -1.1 to -1.9 eV energy interval. The empty Tm 14th *f* energy level is situated around ~ 5.5 eV above the Fermi level hybridized with Tm5*d* states. Seven empty Eu4*f* energy bands are set in the 8.2 to 9.0 eV energy interval (Fig. 16). The spin magnetic moment was found to be $6.87\mu_B$ at the Eu site and $-1.11\mu_B$ at the Tm site, so that the total magnetic moment for formula unit is equal to $5.76\mu_B$ for $\text{Tm}_{0.5}\text{Eu}_{0.5}\text{Se}$, in good agreement with the experimental value of $5.5\mu_B$.³

The theoretically calculated optical reflectivity spectrum of the $\text{Tm}_{0.5}\text{Eu}_{0.5}\text{Se}$ compound shows typical behavior for semiconductor systems with reflectivity equal to 0.17 at zero

frequency. The theoretical spectrum is in good agreement with the experimental measurements by Battlog⁷⁴ (not shown).

The effect of pressure on the transport properties of $\text{Tm}_{0.5}\text{Eu}_{0.5}\text{Se}$ were investigated by Boppert and Wachter.⁷⁵ It was found that at room temperature, the resistivity of $\text{Tm}_{0.5}\text{Eu}_{0.5}\text{Se}$ showed an exponential decrease, indicating a linear closing of the energy gap with transition into the metallic intermediate-valent state.³ In our LSDA+ U band-structure calculations we also found a gradual decreasing of the energy gap with reducing of the lattice constant and the closing of the gap at 5.68 Å in a good agreement with the experiment.³

An interesting case is given by $\text{Tm}_{1-x}\text{Y}_x\text{Se}$, i.e., dilution of TmSe with YSe. YSe has a similar electronic structure as TmSe but with no 4*f* bands. The ionic radius of the Y^{3+} ion corresponds nearly precisely to that of Tm^{3+} , so the first idea was that the Fermi level in the diluted Y compound should be higher than that in TmSe because each Y donates one electron to the conduction band, not just 0.73 as in TmSe. Thus the Fermi level will reach the 13th *f*-hole level, electrons will partially fill this level, and the valency will be shifted towards more divalency.³ However, the real situation is more complicated. We performed the LSDA+ U band-structure calculations for the $\text{Tm}_{0.5}\text{Y}_{0.5}\text{Se}$ compound and found that although, in contrast to TmSe, the empty 14th *f* level in $\text{Tm}_{0.5}\text{Y}_{0.5}\text{Se}$ is shifted towards smaller energies by approximately 0.3 eV, the 13th *f* level is shifted upward and situated at 35 meV above the Fermi level, reminiscent of TmS. Hence, the diluted Y compounds tend toward more trivalency. The explanation of such phenomena is as follows. After substitution for the magnetic Tm ions by nonmagnetic Y ions, long-range antiferromagnetism is suppressed and the system becomes ferromagnetically ordered. Also due to a more attractive ion potential for Y^{3+} in comparison with $\text{Tm}^{2.73+}$, one the 4*d* states of Y is shifted downward relative to the Tm5*d* states. The occupation number of the *d* states is equal to 0.94 in AFM TmSe and 1.11 and 1.41 in FMTm_{0.5}Y_{0.5}Se at the Tm and Y sites, respectively. In other words, the conduction band is filled by *d* electrons to a greater extent in Y-diluted compounds than in TmSe. As a result the occupation of the 13th *f* level is decreased and Y-diluted compounds are shifted towards more trivalency in comparison with TmSe. To clarify the energy position of 13th and 14th *f*-hole levels in the $\text{Tm}_{0.5}\text{Y}_{0.5}\text{Se}$ compound, in optical measurements are highly desired.

IV. SUMMARY

The Tm monochalcogenides TmS, TmSe, and TmTe constitute a very interesting system exhibiting behavior due to strongly correlated electrons. While the standard LSDA approach is unable to correctly describe the electronic structure of these materials because of the strong on-site Coulomb repulsion, U_{eff} , the LSDA+ U approach is remarkably accurate in providing detailed agreement with experiment for a number of properties. In this section we summarize these properties and the results of our work.

In contrast to LSDA, where the stable solution for TmTe is a metal, the LSDA+ U method gave an insulator with an indirect energy gap of 0.58 eV. LSDA+ U theory predicts that the thulium ion in TmTe is in an integer divalent state. It also shows a gradual decreasing of the energy gap with reduction of the lattice constant. The gap is closed at $a = 6.05 \text{ \AA}$, in good agreement with experimental measurements of TmTe transport properties under pressure and the compositionally induced semiconductor-metal transition in the TmSe $_{1-x}$ Te $_x$ system.

For the Tm $^{3+}$ ions of TmS and TmSe twelve $4f$ bands are fully occupied and hybridize with chalcogenide p states. The 14th f -hole level is completely unoccupied and well above the Fermi level. The initially empty hole 13th f level in the process of self-consistent relaxation becomes partly occupied with $4f$ DOS maximum situated in close vicinity of the Fermi level in TmS and TmSe. A fundamental aspect of this observation is that we find the partial occupation of the 13th f state to be a robust property of TmS and TmSe compounds: it happens irrespective of the precise value of U_{eff} . The positions of the 13th and 14th f -hole levels in TmS and TmSe are in good agreement with BIS and optical measurements. The degree of occupation and position of the partly occupied 13th f level with respect to the Fermi level is different in TmS and TmSe. In TmS the hole level is almost empty and situated significantly far from the Fermi level. Such a situation is appropriate for achieving the Kondo lattice scenario. In TmSe the upper hole 13th f level is pinned at the Fermi level, therefore, TmSe is expected to be an intermediate-valent compound in agreement with experimental data. The occupation number of the 13th f -hole level is equal to 0.12 and 0.27 (valency 2.88+ and 2.73+) in TmS and TmSe, respectively, in a good agreement with the experimental estimates from lattice constant and XPS and UPS measurements.

The *ab initio* LSDA+ U theoretical calculations describe well the measured XPS and UPS Tm monohalogenides spectra only after taking into account the multiplet structure of final $4f^{11}$ and $4f^{12}$ states for Tm $^{3+}$ and Tm $^{2+}$ ions, respectively. It was shown that the structures in the XPS and UPS spectra of TmS and TmSe between -4.5 and -16 eV

binding energy should be assigned to the final-state multiplet structure derived from twelve fully occupied $4f$ bands (Tm $^{3+}$) and the structures between 0.0 and -4.5 eV are associated with the final-state multiplet structure of the partly occupied 13th $4f$ state.

In conclusion we have shown that the MO spectra of TmX ($X = \text{S, Se, Te}$) are very sensitive tools for drawing conclusions about the appropriate model description. On account of the calculated MO spectra we conclude that TmS and TmSe MO spectra are best described using the LSDA+ U approach. The shape of the Kerr spectra in TmS and TmSe is mostly due to a resonance structure of the function $[\omega D(\omega)]^{-1}$ due to a steep plasma edge (see Fig. 7). Our analysis indicates that the available experimental Kerr spectra for TmSe $_{0.32}$ Te $_{0.68}$ is a complex mixture of the divalent and trivalent Tm ion spectra.

Our LSDA+ U band-structure calculations support the picture of the electronic structure of TmX ($X = \text{S, Se, Te}$) (except of some minor details) remarkably drawn earlier by Wachter³ using only the experimental data. A remaining important question is: does TmSe exhibit the metal-dielectric or metal-semimetal transition through the FM-AFM phase transition? LSDA+ U theory was not able to produce an energy gap. The appearance of this energy gap may be caused by both hybridization and exciton effects due to the Coulomb attraction of the $5d$ conduction electron and the $4f$ hole. This effect cannot be described in the one-particle approximation. On the other hand, several experimental facts indicate that there might not be a gap but rather a pseudogap. This interesting question requires further investigation theoretically as well as experimentally.

ACKNOWLEDGMENTS

This work was carried out at the Ames Laboratory, which is operated for the U.S. Department of Energy by Iowa State University under Contract No. W-7405-82. This work was supported by the Director for Energy Research, Office of Basic Energy Sciences of the U.S. Department of Energy. V. N. Antonov gratefully acknowledges the hospitality at Ames Laboratory during his stay.

*Permanent address: Institute of Metal Physics, 36 Vernadskii Street, 252142 Kiev, Ukraine.

¹E. Bucher, K. Andres, F. J. di Salvo, J. P. Maita, A. C. Gossard, A. S. Cooper, G. W. Hull, Phys. Rev. B **11**, 500 (1975).

²R. Suryanarayanan, G. Güntherodt, J. L. Freeouf, and F. Holzberg, Phys. Rev. B **12**, 4215 (1975).

³P. Wachter, in *Handbook of the Physics and Chemistry of Rare Earths*, edited by K. A. Gschneidner, L. Eyring, and S. Hufner (North-Holland, Amsterdam, 1994), Vol. 19, p. 177.

⁴Y. Lassailly, C. Vettier, F. Holtzberg, J. Flouquet, C. M. E. Zeyen, F. Lapierre, Phys. Rev. B **28**, 2880 (1983).

⁵A. Berger, E. Bucher, P. Haen, F. Holzberg, F. Lapierre, T. Penney, and R. Tournier, in *Valence Instabilities and Related Narrow Band Phenomena*, edited by R. D. Parks (Plenum, New York, 1977), p. 491.

⁶P. Haen, H. Bioud, F. Lapierre, and F. Holzberg, in *Theoretical and Experimental Aspects of Valence Fluctuations, Proceedings*

of the 5th International Conference on Valence Fluctuations, Bangalore, 1987, edited by L. C. Gupta and S. K. Malik (Plenum, New York, 1987), p. 445.

⁷F. Lapierre, P. Haen, B. Coqblin, M. Ribault, and F. Holzberg, Physica **108B**, 1351 (1981).

⁸J. M. Lawrence, P. S. Riseborough, and R. D. Parks, Rep. Prog. Phys. **44**, 1 (1981).

⁹M. Campagna, G. K. Wertheim, and E. Bucher, *Structure and Bonding* (Springer, Berlin, 1976), Vol. 30, p. 99.

¹⁰M. Campagna, E. Bucher, G. K. Wertheim, D. N. E. Buchanan, and L. D. Longinotti, Phys. Rev. Lett. **32**, 885 (1974).

¹¹G. Kaindl, C. Laubschat, B. Reihl, R. A. Pollak, N. Martensson, F. Holtzberg, and D. E. Eastman, Phys. Rev. B **26**, 1713 (1982).

¹²G. K. Wertheim, W. Eib, E. Kaldis, and M. Campagna, Phys. Rev. B **22**, 6240 (1980).

¹³E. Bucher, K. Andres, F. J. di Salvo, J. P. Maita, A. C. Gossard, A. S. Cooper, and G. W. Hull, Phys. Rev. B **11**, 500 (1975).

- ¹⁴Y. Ufuktepe, S. Kimura, T. Kinoshita, K. G. Nath, H. Kumigashira, T. Takahashi, T. Matsumura, T. Suzuki, H. Ogasawara, and A. Kotani, *J. Phys. Soc. Jpn.* **67**, 2018 (1998).
- ¹⁵B. Batlogg, H. R. Ott, E. Kaldis, W. Thoni, and P. Wachter, *Phys. Rev. B* **19**, 247 (1979).
- ¹⁶P. Haen, F. Lapierre, J. M. Mignot, R. Tournier, and F. Holtzberg, *Phys. Rev. Lett.* **43**, 304 (1979).
- ¹⁷M. Ribault, J. Floquet, P. Haen, F. Lapierre, J. M. Mignot, and F. Holtzberg, *Phys. Rev. Lett.* **45**, 1295 (1980).
- ¹⁸K. Andres, W. M. Walsh, Jr., S. Darack, L. W. Rupp, Jr., and L. D. Longinotti, *Solid State Commun.* **27**, 825 (1978).
- ¹⁹A. Berton, J. Chaussy, B. Cornut, J. Flouquet, J. Odin, J. Peyrard, and F. Holtzberg, *Phys. Rev. B* **23**, 3504 (1981).
- ²⁰F. Holtzberg, T. Penney, and R. Tournier, *J. Phys. (Paris), Colloq.* **40**, C5-314 (1979).
- ²¹E. Kaldis and B. Frizler, *Prog. Solid State Chem.* **14**, 95 (1982).
- ²²P. Hayen, F. Holtzberg, F. Lapierre, T. Penney, and R. Tournier, in *Valence Instabilities and Related Narrow Band Phenomena*, edited by R. D. Parks (Plenum, New York, 1977), p. 495.
- ²³Y. Lassailly, C. Vettier, F. Holtzberg, A. Benoit, and J. Flouquet, *Solid State Commun.* **52**, 717 (1984).
- ²⁴E. Clementyev, R. Köhler, M. Braden, J.-M. Mignot, C. Vettier, T. Matsumura, and T. Suzuki, *Physica B* **230–232**, 735 (1977).
- ²⁵T. Matsumura, T. Kosaka, J. Tang, T. Matsumoto, H. Takahashi, N. Mori, and T. Suzuki, *Phys. Rev. Lett.* **78**, 1138 (1997).
- ²⁶P. Wachter, *J. Magn. Magn. Mater.* **31–34**, 439 (1983).
- ²⁷H. Launois, M. Rawiso, E. Holland-Moritz, R. Pott, and D. Wohlleben, *Phys. Rev. Lett.* **44**, 1271 (1980).
- ²⁸P. Wachter, S. Kamba, and M. Grioni, *Physica B* **252**, 178 (1998).
- ²⁹B. Batlogg, *Phys. Rev. B* **23**, 1827 (1981).
- ³⁰P. Wachter, F. Bommeli, and M. Filzmoser, *Solid State Commun.* **108**, 641 (1998).
- ³¹W. Reim, J. Schoenes, and O. Vogt, *Phys. Rev. B* **29**, 3252 (1984).
- ³²J. Schoenes, W. Reim, *J. Less-Common Met.* **112**, 19 (1985).
- ³³W. Reim and J. Schoenes, in *Ferromagnetic Materials*, edited by E. P. Wohlfarth and K. H. J. Buschow (North-Holland, Amsterdam, 1990), Vol. 5, p. 133.
- ³⁴H. J. F. Jansen, A. J. Freeman, and R. Monnier, *J. Magn. Magn. Mater.* **47–48**, 459 (1985).
- ³⁵A. I. Lichtenstein and M. I. Katsnelson, *Phys. Rev. B* **57**, 6884 (1988).
- ³⁶V. N. Antonov, V. P. Antropov, B. N. Harmon, A. N. Yaresko, and A. Ya. Perlov, *Phys. Rev. B* **59**, 14 552 (1999).
- ³⁷V. N. Antonov, B. N. Harmon, A. Ya. Perlov, and A. N. Yaresko, *Phys. Rev. B* **59**, 14 561 (1999).
- ³⁸V. N. Antonov, B. N. Harmon, A. N. Yaresko, and A. Ya. Perlov, *Phys. Rev. B* **59**, 14 571 (1999).
- ³⁹V. N. Antonov, B. N. Harmon, V. P. Antropov, A. Ya. Perlov, and A. N. Yaresko (unpublished).
- ⁴⁰V. I. Anisimov, J. Zaanen, and O. K. Andersen, *Phys. Rev. B* **44**, 943 (1991).
- ⁴¹V. V. Nemoshkalenko and V. N. Antonov, *Computational Methods in Solid State Physics* (Gordon and Breach, London, 1998).
- ⁴²L. Hedin and B. I. Lundqvist, *J. Phys. C* **4**, 2064 (1971).
- ⁴³F. Aryasetiawan and O. Gunnarsson, *Rep. Prog. Phys.* **61**, 237 (1998).
- ⁴⁴V. I. Anisimov, F. Aryasetiawan, and A. I. Lichtenstein, *J. Phys.: Condens. Matter* **9**, 767 (1997).
- ⁴⁵P. M. Oppeneer, V. N. Antonov, A. N. Yaresko, A. Ya. Perlov, and H. Eschrig, *Phys. Rev. Lett.* **78**, 4079 (1997).
- ⁴⁶V. N. Antonov, A. N. Yaresko, A. Ya. Perlov, P. Thalmeier, P. Fulde, P. M. Oppeneer, and H. Eschrig, *Phys. Rev. B* **58**, 9752 (1998); H. Eschrig, V. N. Antonov, A. N. Yaresko, A. Ya. Perlov, P. Thalmeier, P. Fulde, and P. M. Oppeneer, *Physica B* **259–261**, 267 (1999).
- ⁴⁷A. I. Lichtenstein, V. P. Antropov, B. N. Harmon, *Phys. Rev. B* **49**, 10 770 (1995); A. N. Yaresko, P. M. Oppeneer, A. Ya. Perlov, V. N. Antonov, T. Kraft, and H. Eschrig, *Europhys. Lett.* **36**, 551 (1996); D. L. Price, B. R. Cooper, S. P. Lim, and I. Avgin, *Phys. Rev. B* **61**, 9867 (2000).
- ⁴⁸P. Villars and L. D. Calvert, *Pearson's Handbook of Crystallographic Data for Intermetallic Phases* (ASM International, Materials Park, 1991).
- ⁴⁹U. von Barth and L. A. Hedin, *J. Phys. C* **5**, 1692 (1972).
- ⁵⁰O. K. Andersen, *Phys. Rev. B* **12**, 3060 (1975); D. D. Koelling and B. N. Harmon, *J. Phys. C* **10**, 3107 (1977).
- ⁵¹V. V. Nemoshkalenko, A. E. Krasovskii, V. N. Antonov, V. N. Antonov, U. Fleck, H. Wonn, and P. Ziesche, *Phys. Status Solidi B* **120**, 283 (1983).
- ⁵²V. N. Antonov, A. Ya. Perlov, A. P. Shpak, and A. N. Yaresko, *J. Magn. Magn. Mater.* **146**, 205 (1995).
- ⁵³H. Ebert, *Phys. Rev. B* **38**, 9390 (1988).
- ⁵⁴V. N. Antonov, A. I. Bagljuk, A. Ya. Perlov, V. V. Nemoshkalenko, V. N. Antonov, O. K. Andersen, and O. Jepsen, *Low Temp. Phys.* **19**, 494 (1993).
- ⁵⁵P. E. Blöchl, O. Jepsen, and O. K. Andersen, *Phys. Rev. B* **49**, 16 223 (1994).
- ⁵⁶J. F. Herbst and J. W. Wilkins, in *Handbook of the Physics and Chemistry of Rare Earths*, edited by K. A. Gschneidner, L. Eyring, and S. Hüfner (North-Holland, Amsterdam, 1987), Vol. 10, p. 321.
- ⁵⁷P. H. Dederichs, S. Blügel, R. Zeller, and H. Akai, *Phys. Rev. Lett.* **53**, 2512 (1984).
- ⁵⁸V. I. Anisimov and O. Gunnarsson, *Phys. Rev. B* **43**, 7570 (1991).
- ⁵⁹H. B. Moller, S. M. Shapiro, and R. J. Birgeneau, *Phys. Rev. Lett.* **39**, 1021 (1977).
- ⁶⁰E. Holland-Moritz and G. H. Lander, in *Handbook of the Physics and Chemistry of Rare Earths*, edited by K. A. Gschneidner, L. Eyring, and S. Hüfner (North-Holland, Amsterdam, 1994), Vol. 19, p. 1.
- ⁶¹J. J. Yeh and I. Lindau, *At. Data Nucl. Data Tables* **32**, No. 1 (1985).
- ⁶²P. A. Cox *Structure and Bonding*, 24 (Springer, Berlin, 1975), p. 59.
- ⁶³G. Racah, *Phys. Rev.* **76**, 1352 (1949).
- ⁶⁴H. S. Bennet and E. A. Stern, *Phys. Rev.* **137**, A448 (1965).
- ⁶⁵M. Rohlfing and S. G. Louie, *Phys. Rev. B* **62**, 4927 (2000).
- ⁶⁶H. Feil and C. Haas, *Phys. Rev. Lett.* **58**, 65 (1987).
- ⁶⁷L. L. Hirst, *Phys. Kondens. Mater.* **11**, 255 (1970).
- ⁶⁸C. M. Varma, *Rev. Mod. Phys.* **48**, 219 (1976).
- ⁶⁹F. Marabelli and P. Wachter, in *Theoretical and Experimental Aspects of Valence Fluctuations and Heavy Fermions*, edited by L. C. Gupta and S. K. Malik (Plenum, New York, 1987), p. 269.

- ⁷⁰A. Amato and J. Sierro, *J. Magn. Magn. Mater.* **47–48**, 475 (1985).
- ⁷¹B. Batlogg, A. Schlegel, and P. Wachter, *Physica B* **86–88**, 229 (1977).
- ⁷²H. Boppart, *J. Magn. Magn. Mater.* **47–48**, 436 (1985).
- ⁷³E. Kaldis, B. Fritzler, E. Jilek and A. Wisard, in *Valence Instabilities*, edited by P. Wachter (New-Holland, Amsterdam, 1982), p. 131.
- ⁷⁴B. Batlogg, *Phys. Rev. B* **23**, 650 (1981).
- ⁷⁵H. Boppart and P. Wachter, in *Physics of Solids under High Pressure*, edited by J. S. Schilling and R. N. Shelton (North-Holland, Amsterdam, 1981), p. 301.